Journal of Rock Mechanics and Geotechnical Engineering. 2011, 3 (Supp.): 407–414

Journal of Rock Mechanics and Geotechnical Engineering

Journal online: www.rockgeotech.org

Effect of strata properties and panel widths on chock performance

Manoj Khanal*, Deepak Adhikary, Rao Balusu

Earth Science and Resource Engineering, Commonwealth Scientific and Industrial Research Organization (CSIRO), Queensland Center for Advanced Technology, 1 Technology Court, Pullenvale, QLD 4069, Australia

Received 7 December 2010; received in revised form 3 May 2011; accepted 13 July 2011

Abstract: The selection of optimum chock (support) capacity is very crucial for a successful longwall mining. The selection of chock capacity depends on the site-specific geotechnical parameters, constraints and longwall panel geometry, which are generally not known in detail in priority. Hence, based on the field and laboratory data, various possible combinations should be analyzed to cater for the unforeseeable mining conditions. This paper discusses the use of numerical model for selecting an appropriate chock capacity based on the site-specific geological and geotechnical information and longwall panel geometry. The fracture mechanisms of immediate and main roofs are also discussed for various panel widths and support capacities. For the models considered, the chock convergence is predicted to increase by about 33% due to the increase in face width from 100 to 260 m. Similarly, the massive roof strata are found to yield higher chock convergence compared to bedded strata.

Key words: chock capacity; longwall; simulation; underground mining

1 Introduction

In longwall mining, the choice of roof support system is critical for successful mining operations. It is vital to understand the response of support capacity under local geotechnical conditions in order to select the adequate support capacity for a site-specific mining environment.

Poor ground condition as well as poor choice of longwall support may cause severe face instability problems. It is important to understand the causes of face instability and evaluate the consequences of insufficient support capacity. Support design is based primarily on the replacement of extracted coal with mechanized support capable of controlling the deformation in immediate roof. The support design should also be of sufficient capacity to allow effective mechanized extraction at the desired production rate.

The factors affecting support selection are listed as follows: thickness and strength of immediate roof above the supports (easily caving or massive); strength and thickness of overlaying main strata, especially the information on any unit that may bridge; strength of floor strata; support design and capacity to prevent spalling of face or weakness of roof between tip and face area; alignment of jointing or cleating in the face area; and cutting height.

Over the years, the coal mining industry has made a substantial progress towards better control and management of longwall faces and roofs. Face width of 250 m has become general in Australian mines. The current trend is to use face widths in excess of 300 m wherever feasible.

The level of productivity is influenced by both face width and cutting height, and above average performance indicates possible favourable mining conditions. In general, supports with the capacity of 8–11 MN are being used in mines. Some of the mines have mixed supports with different capacities. Recently, a mine in Australia has introduced 18 MN supports to mitigate the poor ground conditions encountered.

In average, mining height of 3.5 m is common at present for most of the underground mines although there are reports on extracting 7 m thick seam [1]. The efficiency can be improved by increasing the extraction heights. However, due to the machinery limitations and geotechnical constraints, the extraction

Doi: 10.3724/SP.J.1235.2011.00407
*Corresponding author. Tel: +61-7-33274199;
E-mail: Manoj.Khanal@csiro.au

height is often limited. Higher extraction heights can cause instabilities in the faces. The physical size of equipments, the problems of working face transfer, roof control and collapsing of faces, as well as the problems of gate road dimensions and support, are considered to be the major constraints on extending the limit of full-face longwall [2].

Increase in panel widths also increases the production. However, it may create geotechnical and stability problems in addition to the capital cost. The wider panels show more deflection at the centre of the panel, and may cause relatively severe failure compared to the shorter panels. The selection of panel widths also depends on the chock capacities employed and geotechnical constraints of the mine.

Higher support capacities can provide safer mining environments at the cost of capital investment, but this may not be always true [3]. For a given strata condition, peak face convergence gradient increases significantly if an excessively higher capacity of support is deployed at the face [3]. Depending on the geotechnical and overburden properties, convergences of the chocks vary [3, 4]. Mining, as a very competitive industry, is not always desirable to choose the biggest and best support but to choose the optimum capacity and type of support for the given conditions [4].

Selection of optimum capacity of chock is very crucial for a successful mining operation. In this regard, this paper discusses how the properties of overlaying sandstone and width of longwall panels affect the chock capacity selection by using three-dimensional (3D) mine-scale numerical simulations. Meanwhile, the fracture mechanism of immediate roof is discussed for various panel widths and support capacities.

2 Model development

An in-house 3D finite element code coupling stress and deformation with two-phase fluid flow, COSFLOW, which uses the Cosserat continuum theory, is used in this study. A brief description of COSFLOW is provided in Refs.[5–7].

2.1 Model calibration and validation

The available mine data were to calibrate and validate the model used to predict the mine parameters for new mine designs at the same mine site. The field monitoring data were used to calibrate the input parameters from the mine site.

The new mines are planned at the same site where an existing mine is located, hence the model parameters can be calibrated with the existing mine data. A calibration model is developed with an area of approximately 52 km^2. It is necessary to use such a large area to negate any boundary effect. A plan view of the model is shown in Fig.1. All together four longwall panels are simulated. Panels 1–4 are 154, 122, 139 and 160 m wide, respectively, with the same length of 1 017 m. The roadways on both sides of panel 4 are modeled with a width of 4 m.

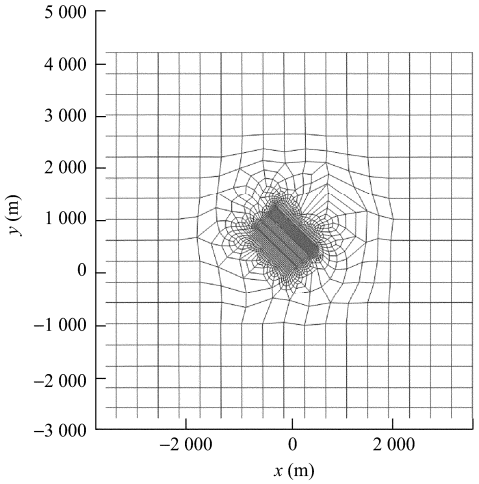

Fig.1 Plan view of the model.

Field monitoring systems (load cells and tell tales) were installed in panel 4 at the mine site, as shown in Fig.2. Layout of monitoring equipments is also shown in Fig.2. Typical mine site data from the load cells are presented in Fig.3. It can be seen that the loads start to increase as the longwall face approaches the load cell positions; and a sharp increase in loads on the load cells occurs once the longwall face is about 10 m away from the load cell positions. A gentle increase in loads occurs when the longwall face is more than 10 m away. It is either due to a possibility that the load cells are not in complete contact with the roof thus yielding a less stiff response to roof deformation, or due to a possibility that the roof deforms only marginally thus not generating significant loads on the load cells.

Figure 3 also shows a comparison of model predicted loads and those measured by the load cells. It can be observed that the model predicts a slow increase in loads when the longwall face is more than 10 m away; and the loads are predicted to increase sharply once the longwall face is less than 10 m away. The model predicts a maximum load of 23 MPa, which agrees well with the field measurement. It can be noted that the roadway roof deforms only marginally until

the longwall face is about 10 m away from the

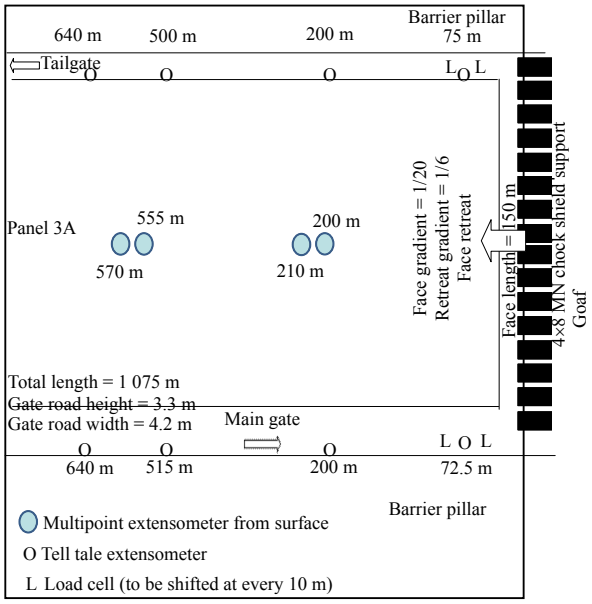

Fig.2 Layout of monitoring system installed at panel 4.

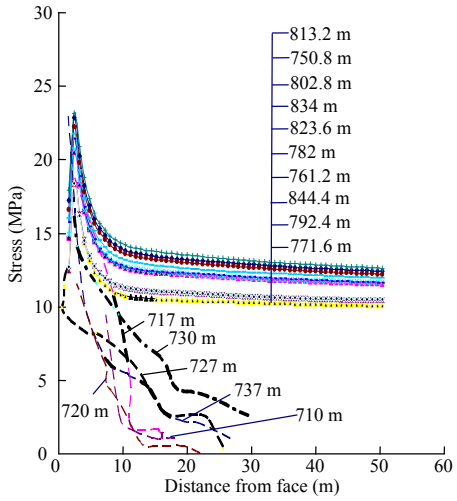

Fig.3 Comparison of COSFLOW results with load cell data obtained from the main gate of panel 4 (broken lines represent measured data, and solid lines with data points represent COSFLOW results).

load cell positions. The stress value of about 10 MPa predicted by the model is mainly due to the extraction of roadways itself and hence would have existed before the start of longwall retreat when the longwall face is more than 10 m away. Since the load cells were installed in the pre-existing roadways in panel 4, the initial load cell readings can be considered as the build-up of initial pressure applied during the installation of hydraulic props.

The quantitative agreement of mine data and modeled data provides a confidence in the model parameters used for the simulations. Thus, the calibrated models and verified input parameters are used to predict the mine parameters for a new mine design at the same mine site.

2.2 New mine models

A plan view of the model can be seen in Fig.4, in which panel 1 is 260 m wide and 2 065 m long, and panel 2 is also 260 m wide and 2 402 m long. A 40 m wide chain pillar is adopted.

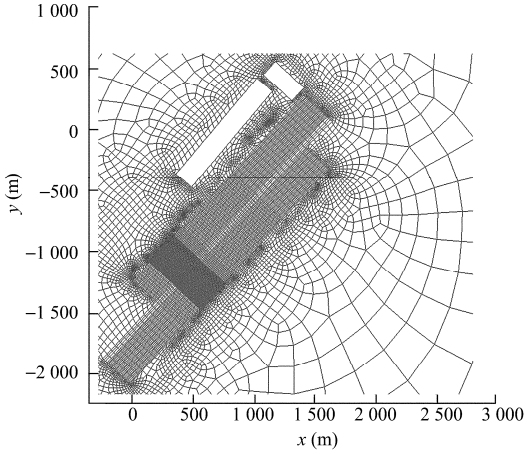

Fig.4 Plan view of the discretized model.

A typical core log of the model is shown in Fig.5. The extracted thickness of a coal seam is 3.3 m. The longwall panels were extracted in steps to minimize shock loading to the model. The panels were excavated in decreasing step sizes for a distance of 600 m from the start-up line. After this, chocks were installed and further extracted for an additional distance of 250 m.

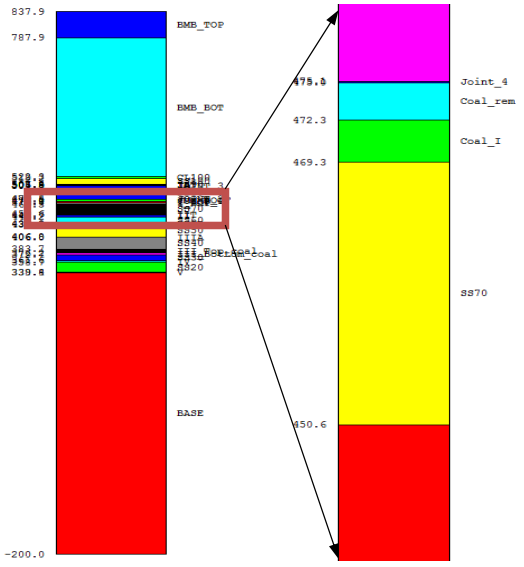

Fig.5 A typical core log of the model (unit: m).

The perfectly elastoplastic Mohr-Coulomb model was employed in the constitutive models for the rock blocks and joints. The roller boundaries were prescribed on the four sides and the base of the model. Initial stress field equal to the in-situ stresses measured at the mine site was prescribed. Tables 1 and 2 provide the strength values used in the numerical model for various strata in different cases. These five models based on various material properties are selected to provide a range of strengths, which could be encountered in a new ground. They represent an array of strengths varying from the weakest to strongest ground conditions so that the model can simulate the strata close to practical cases.

Table 1 Rock mass strength values for base case (case 1).

Layer	Density (kg/m^3)	σ_T (MPa)	E (GPa)	φ (°)	ν	K (GPa)	G (GPa)	c (MPa)	ψ (°)
BMB	2 045	0.25	3.7	31.42	0.2	2.06	1.54	0.7	5
SS100	2 172.06	0.68	7.14	40.71	0.2	3.9	2.98	1.55	5
SS80	2 125.09	0.61	6.07	41.56	0.19	3.31	2.54	1.38	5
COAL	1 496.7	1.35	3	40	0.12	1.32	1.34	1.24	7.5
SS70	2 246.56	0.98	7.43	40.43	0.2	4.18	3.09	2.27	5
SS60	2 192.46	0.75	7.17	35.54	0.14	3.33	3.14	1.94	5
SS50	2 234.11	0.78	6.66	39.82	0.18	3.43	2.83	1.83	5
SS40	2 187.49	0.58	5.7	39.35	0.19	3.09	2.39	1.37	5
SS30	2 248.65	0.84	7.96	45.5	0.24	5.05	3.22	1.71	5
SS20	2 196.63	0.81	8.96	42.79	0.22	5.36	3.67	1.76	5
BASE	1 957.36	0.94	5.35	39.48	0.18	3.17	2.26	4.72	6.19

Note: the sandwiched (not extracted) coal and clay layers are not listed.

Table 2 Values of cohesion of rock mass for different cases.

MPa

Layers	Case 1 (base case)	Case 2	Case 3	Case 4	Case 5
SS100	1.55 (layered)	2.82 (layered)	1.55 (massive)	1.55 (layered)	3.1 (massive)
SS80	1.46 (massive)	2.93 (massive)	1.46 (massive)	1.46 (layered)	2.93 (massive)
SS70	1.27	3.62	1.27	1.27	3.62
SS60	1.94	3	1.94	1.94	3
SS50	1.83	2.79	1.83	1.83	2.79
SS40	1.46	2.14	1.46	1.46	2.14
SS30	1.71	2.41	1.71	1.71	2.41
SS20	1.76	2.81	1.76	1.76	2.81

Case 1 represents the base case with the properties shown in Table 2. In this case, SS80 and SS100 were massive and layered, respectively. The planes of weaknesses were introduced on the top and bottom of SS80.

In case 2, the rock mass strength was increased for all the rock units except for SS80. The strength of SS80 was double that of the base case. The planes of weaknesses were again introduced on the top and bottom of SS80.

In case 3, the rock mass strengths of all the rock units were kept the same as those of case 1. However, both SS80 and SS100 were kept massive and the planes of weaknesses were introduced on the top and bottom of SS80 and SS100.

Case 4 was similar to case 1 except that the SS80 unit was layered.

Case 5 represents an extreme condition where the rock mass strength was increased for all the rock units except for SS80 and SS100. The rock mass strengths of SS80 and SS100 were double that of base case, and were also massive. The planes of weaknesses were introduced on the top and bottom of SS80 and SS100.

Four different panel widths (i.e. 260, 200, 160 and 100 m) and two different chock capacities (i.e. 8 and 11 MN) were simulated to study the variation in strength properties of SS80 (main roof) and SS100, as shown in Table 3.

Table 3 Different chock capacities and panel widths modeled in this study.

Panel width (m)	Material variation	Chock capacity	
		8 MN	11 MN
100	Case 1	—	√
	Case 3	—	√
	Case 5	—	√
160	Case 1	—	√
	Case 3	—	√
	Case 4	—	√
	Case 5	—	√
200	Case 1	—	√
	Case 2	—	√
	Case 3	—	√
	Case 4	—	√
	Case 5	—	√
260	Case 1	√	√
	Case 2	√	√
	Case 5	√	√

The chocks were modeled as hexahedral elements. The deformation at each node of the elements was noted and averaged out to calculate the average deformation of hexahedral elements. The element expansion and shrinkage were also noted and considered in the averaging process. The average deformation of elements was considered as chock convergence.

In general, the time-dependent effects on caving and support loading are complex and cannot be well

understood. The available computer power restricts the use of a fully dynamic 3D model to study the roof-support interaction mechanism in detail. Thus, the COSFLOW models used in this study are static models, i.e. the models do not consider time effect on roof deformation and its impact on chock convergence. However, the 3D COSFLOW models are expected to yield reliable estimations of periodic weighting and indications of chock convergence, which can be used for qualitative assessment of effect of different mine geometries and strata properties.

3 Results and discussion

3.1 Chock convergence

3.1.1 *Effect of massive and bedded strata*

Figure 6 presents a comparison of convergences of 11 MN chock in a 200 m wide panel with massive SS80 unit and bedded SS80 unit (i.e. cases 1 and 4). Extraction of the first panel is considered here. In general, the bedded roof (case 4) can be seen to yield a smaller convergence compared to the massive roof (case 1).

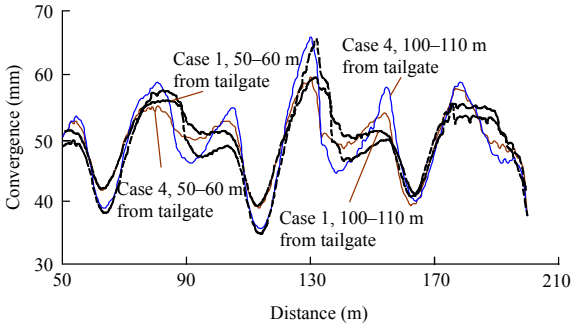

Fig.6 Convergence of 11 MN chock in 200 m wide panel for cases 1 and 4 (panel 1, massive and bedded SS80 unit).

The convergence data from Fig.6 clearly show the periodic loading on the chocks. Two types of periodic loadings could be seen. The massive strata model shows a longer periodic weighting cycle compared to the bedded strata model. The bedded strata model can be seen to exhibit two distinct periodic loading patterns. The milder periodic loading is predicted to occur every 15–20 m while the major one is predicted to occur every 30–65 m. In a normal mining situation, the rock strata properties are expected to vary within the mining block as well as within a panel. Thus the actual convergence and the periodic weighting interval are expected to lie within those predicted for cases 1 and 4.

3.1.2 *Effect of strata strength*

Figure 7 shows the convergence of 11 MN chock in a 200 m wide panel for cases 3 and 5. The rock units SS80 and SS100 are stronger in case 5 and subsequently the convergences can be seen to be higher in case 5 compared to those in case 3. Since SS80 and SS100 are massive, the milder repeated loadings are not presented.

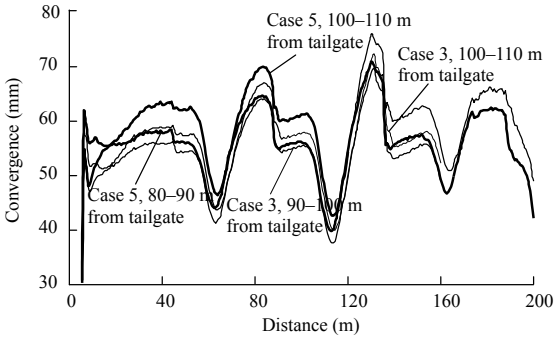

Fig.7 Convergence of 11 MN chock in 200 m wide panel for cases 3 and 5 (panel 1, massive SS80, additional planes of weaknesses on top and bottom of SS100).

The maximum convergence observed in case 5 is 78 mm, which is approximately 7 mm higher than that in case 3. During simulations, similar observation was noted for 160 m wide panels for cases 3 and 5 with 11 MN chock.

Figure 8 presents the convergence of 11 MN chock in a 260 m wide panel for cases 1 and 2, respectively. The chock convergences are given for both panels 1 and 2. For panel 1 in case 1, the chock convergence can be seen to fluctuate at around 42 mm at a distance

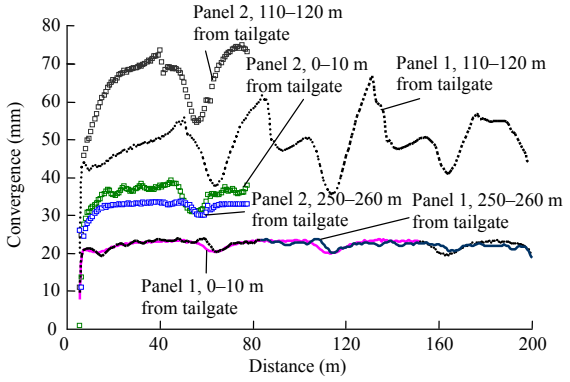

(a) Case 1.

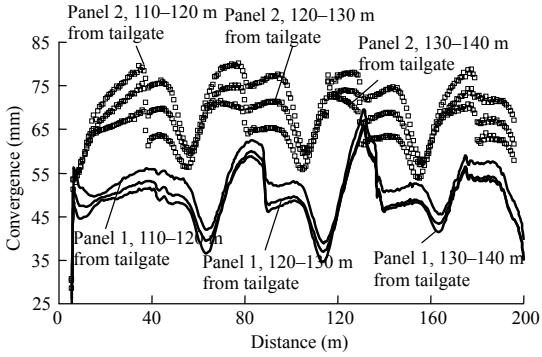

(b) Case 2.

Fig.8 Convergence of 11 MN chock in 260 m wide panel for cases 1 and 2.

of 110–120 m from the tailgate, whereas for panel 2 the chock convergence can be seen to be around 60 mm. Similar to case 2, the average convergence of panel 1 is around 45 mm and that of panel 2 is around 65 mm. The convergence data clearly show the periodic weighting on the chocks. Again two types of periodic loadings could be seen in Fig.8. The milder periodic loading is predicted to occur every 15–20 m, while the major one is predicted to occur every 45–65 m.

Figure 9 presents the comparison of different cases in a 200 m wide panel with 11 MN chock. It can be seen that case 5, which has the strongest material properties among the simulated cases, shows a maximum chock convergence. Subsequently, cases 3, 2, 1 and 4 show a smaller convergence, though the differences in the latter three seem minimal.

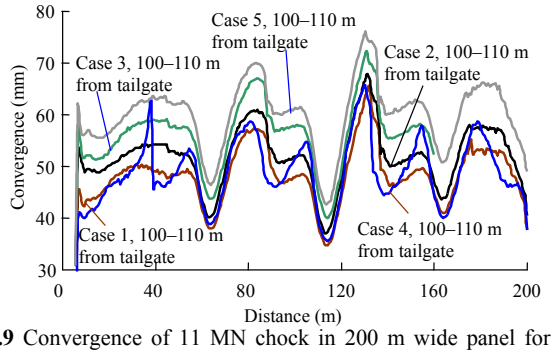

Fig.9 Convergence of 11 MN chock in 200 m wide panel for different cases.

For the considered models, these observations infer two points: (1) Chock convergence is likely to be higher for panels with massive and stronger sandstone units. In cases 3 and 5, SS80 and SS100 are massive and case 5 has the highest strength. Hence, case 5 shows a maximum convergence. Case 2 has a higher rock mass strength for SS80 but has a layered SS100. In case 4, SS80 and SS100 are massive. Subsequently, case 4 shows a higher convergence than case 2. (2) If the strength of each rock unit in the geological model is identical, the massive nature of rock unit will yield higher convergence. This is shown by the chock convergence observed in cases 4 and 1. SS80 and SS100 are layered in case 4, whereas only SS100 is layered in case 1. Hence, case 4 has yielded smaller convergence than case 1.

3.1.3 *Effect of panel width*

A comparison among the chock convergence in 260, 200, 160 and 100 m wide panels for case 1 under 11 MN chock is presented in Fig.10. Due to the varying width of panels, it is not realistic to compare the

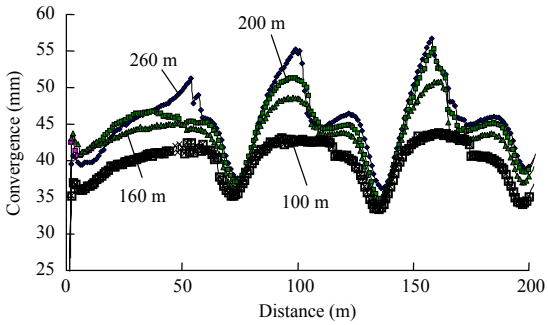

Fig.10 Comparison of different width panels for case 1 with 11 MN chock.

chock convergence at a particular distance from the tailgate. Hence, the average values of chock convergence along the width of the panels are computed and plotted in Fig.10. The maximum average chock convergence for 260, 200, 160 and 100 m panels is around 54, 52, 46 and 36 mm, respectively. It can be seen from Fig.10 that, as the width of the panel decreases, the difference in average chock convergence increases, which is around 33% between 260 and 100 m wide panels.

3.2 Strata caving behavior

The overlaying sandstone units such as SS80 and SS100 both could have an impact on face and chock loading. Thus, in addition to chock convergence analyses, the study also aims at better understanding of deformation behavior of overlaying strata, especially for SS80 and SS100 sandstone units.

Figure 11 presents comparative yield plots of SS80 and SS100 units for different longwall distances noted in each subfigure. These subfigures present the results obtained for case 5 with 11 MN chock in 260, 200, 160 and 100 m wide panels, respectively. It is noted that in case 5, both SS80 and SS100 are assumed to be massive and the strength of overlaying rock units is the strongest among different cases. In Fig.11, except for the case of zero yield (i.e. rock never yields or fractures and remains elastic), all other values indicate that the rock fails.

For SS80 unit, Fig.11 clearly indicates that SS80 would cave in without much difficulty. It is interesting to note that in most of the cases, the failure of SS80 is lagging behind the face line by a certain distance.

Apart from the 100 m wide panel, the SS80 yield zone seems to extend to sideways above the chain pillars. However, it is worthwhile to note that the model is static in nature, and it does not consider the time-dependent deformation. This infers that the caving of

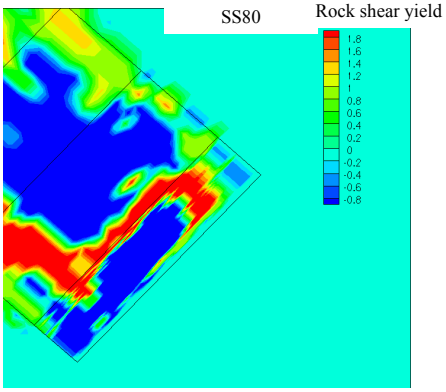

1 721 m (1 665+56) from the face line

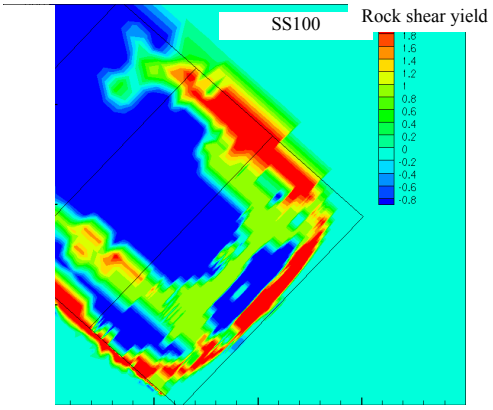

1 783.4 m (1 665+118.4) from the face line

(a) 260 m.

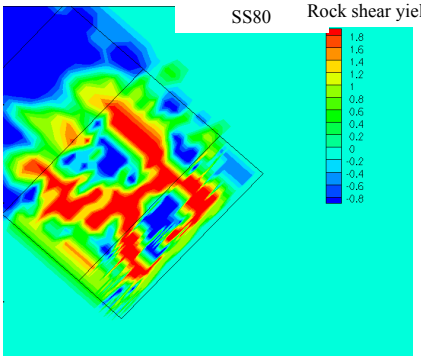

1 721 m (1 665+56) from the face line

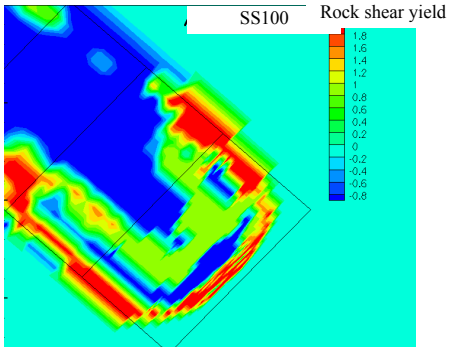

1 757.8 m (1 665+92.8) from the face line

(b) 200 m.

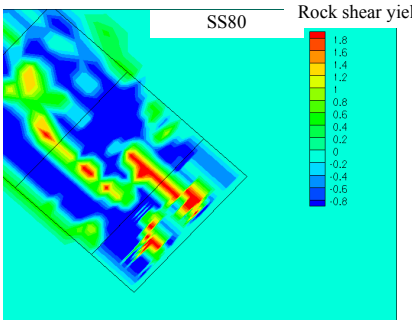

1 721 m (1 665+56) from the face line

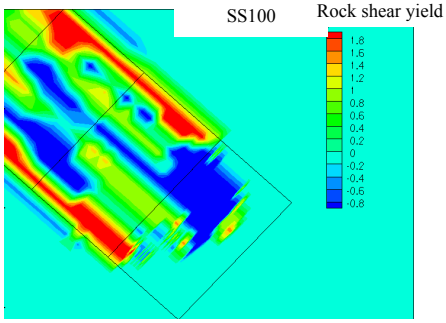

1 779.4 m (1 665+114.4) from the face line

(c) 160 m.

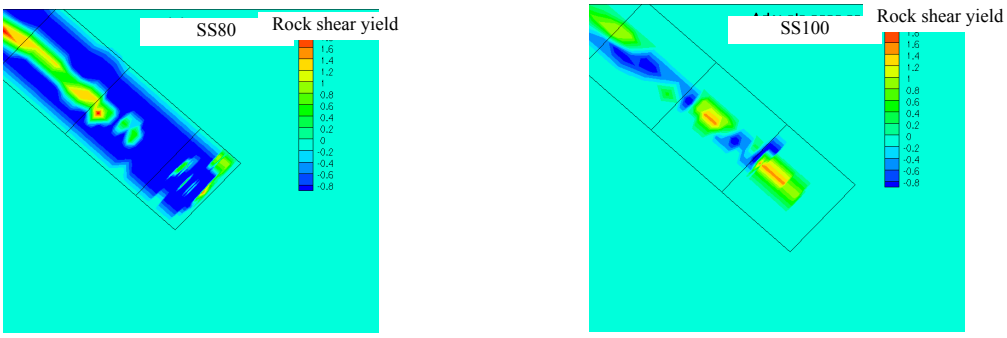

1 721 m (1 665+56) from the face line

1 761.8 m (1 665+96.8) from the face line

(d) 100 m.

Fig.11 SS80 and SS100 caving for different panel widths (panel 1) extraction.

SS80 could possibly occur after a couple of cuts, and fracturing of SS80 could extend all the way to the face line if the mining is stopped for an extended period (i.e. for a couple of hours).

The evolution of fracturing in SS100 unit seems to take arch shapes and lag substantially behind the face line. This distance between the fracture front and the face line seems to increase with the decrease in panel width.

For 100 m wide panels, the plots can be seen to be different from those obtained for the case of 160, 200, and 250 m wide panels. It clearly shows that in this case, SS100 unit will only partially crack (i.e. not cave in completely) and will pass fewer loads on the chocks, resulting in smaller chock convergence, as shown in Fig.10. It indicates that the predicted main cyclic loading is mainly caused by the deformation and fracturing in SS100 unit.

For panels with the width no less than 160 m, compared to the fracturing patterns of SS80, the fracturing of SS100 seems to be more compart-mentalised and shows three distinct bands, i.e. one is located towards the tailgate, one located in the panel centre, and the last one is located towards the main gate. The fracturing in the panel centre is predicted to advance further than the one located towards the tailgate side, followed by the one located toward the main gate side. All the fracturing is predicted to occur behind the chocks.

A number of important observations can be made from Fig.11: (1) In comparison with the fracturing in SS80, the fracture front in SS100 seems to take arch shapes and lag substantially behind the face line. This distance between the fracture front and the face line seems to increase with the decrease in panel width. (2) The fracturing of SS100 appears to be compartmentalised along the mining direction and concentrated more towards the main gate side, which may be attributed to the dipping seam.

4 Conclusions

(1) The chock convergence is predicted to increase by about 33% due to the increase in face width from 100 to 260 m. The difference in the chock convergence between 260, 200 and 160 m wide panels is marginal. As anticipated, the assumption of massive strata compared to bedded strata has yielded higher chock convergence.

(2) The simulations predict a relatively small difference in convergence magnitudes between 8 and 11 MN models, indicating that chocks with capacity in excess of 8 MN would suffice in normal situations. However, longwall operations are likely to encounter adverse geotechnical conditions (such as faulting, strong and hard to cave sandstone channels, etc.) from time to time. In those circumstances, it would be desirable to have extra support capacities to successfully pass through the difficult section.

(3) The analyses of strata caving for different face widths indicate SS80 would cave in easily but probably with some delays. The SS100 would develop an arch-shaped failure and is located behind the chock giving a favorable mining condition. The stronger and massive immediate sandstones (SS80 and SS100, cases 3 and 5) would cave in with a less favorable manner than the weaker cases (cases 1, 2 and 4). The 250 and 200 m wide faces will cause both SS80 and SS100 units to fracture more severely than 100 and 160 m wide panels. This could contribute to extra loading on the chocks, which could be related to higher chock convergence.

Acknowledgement

The authors would like to acknowledge the Singareni Collieries Company Ltd. for providing the data and permission to publish this paper.

References

[1] Li Zhijun, Song Xuanmin, Fu Yuping, Xing Pingwei. Optimizing selection of mining method for extra-thick coal seams in Shendong mining area. Mining Research and Development, 2010, (3): 10–12 (in Chinese).

[2] Ghosh A. Underground methods of extraction of thick coal seams—a global survey. Mining Science and Technology, 1984, 2 (1): 17–32.

[3] Singh G S P, Singh U K. Prediction of caving behaviour of strata and optimum rating of hydraulic powered support for longwall workings. International Journal of Rock Mechanics and Mining Sciences, 2010, 47 (1): 1–16.

[4] Porter I, Aziz N I. Loongwall facelines: geology, convergence and powered support rating. Mining Science and Technology, 1988, 6 (7): 243–252.

[5] Adhikary D P, Dyskin A V. A Cosserat continuum model for layered media. Computers and Geotechnics, 1997, 20 (1): 15–45.

[6] Adhikary D P, Guo H. An orthotropic Cosserat elastoplastic model for layered rocks. Rock Mechanics and Rock Engineering, 2002, 35 (3): 161–170.

[7] Cosserat E, Cosserat F. Theorie des corps deformables. Paris: [s. n], 1909 (in French).